Journal of Colloid and Interface Science 646 (2023) 663–670

Contents lists available at ScienceDirect

Journal of Colloid And Interface Science

journal homepage: www.elsevier.com/locate/jcis

Electroless Deposition of Silver onto Silica Nanoparticles to Produce Lipophilic Core-Shell Nanoparticles

Matthew David Brucks, Alina Arslanova, Caroline Bridget Smith, Jeffrey John Richards *

Department of Chemical and Biological Engineering, Northwestern University, Evanston, IL 60208, USA

HIGHLIGHTS

- Modified electroless deposition of silver onto silica with a lipophilic surface coating.
- Poloxamer surfactant temporarily stabilizes lipophilic particles during aqueous synthesis.
- Amine-terminated alkanes used as capping agents reduce particle sedimentation by controlling tail architecture.
- Capping agent and template concentration control silver shell morphology.
- Synthesis can be performed with varying template geometry.

GRAPHICAL ABSTRACT

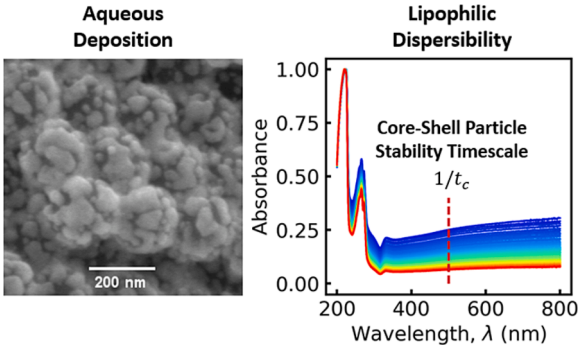

ARTICLE INFO

Keywords:
Lipophilic core–shell nanoparticles
Electroless plating
Capping agent
Colloidal stability
Shell morphology
Amine-terminated alkane
Silver

ABSTRACT

Hypothesis: The colloidal stability of noble metal nanoparticles can be tuned for solvents of varying hydrophobicity by modifying the surface chemistry of the particles with different capping agent architectures. Challenges arise when attempting to separately control multiple nanoparticle properties due to the interdependence of this adsorption process on the surface chemistry and metal architecture. A surfactant-mediated, templated synthesis strategy should decouple control over size and stability to produce lipophilic nanoparticles from aqueous reagents.

Experiments: A modified electroless plating process that produces oil-dispersible core–shell silver-silica nanoparticles is presented. Amine-terminated alkanes are utilized as the capping agents to generate lipophilic surface coatings and the particles are temporarily stabilized during the synthesis by adding a Pluronic surfactant that enhances dispersibility in the aqueous reaction medium. The evolution of shell morphology, composition, and colloidal stability was analyzed against capping agent architecture and concentration. The role of particle shape was also tested by interchanging the template geometry.

Abbreviations: AgSiNP, core-shell silver-silica nanoparticle; Ag, silver; SiNP, silica nanoparticle; SiNR, silica nanorod; TFA, trifluoroacetic acid; TEOS, tetraethyl orthosilicate; KOH, potassium hydroxide; P407, poloxamer 407; SDS, sodium dodecyl sulfate; Brij-35, polyoxyethylene lauryl ether; HRSEM, high resolution scanning electron microscopy; DLS, dynamic light scattering; UV–vis, UV–Visible spectroscopy; XRD, X-ray diffraction; $SnCl_2$, tin (II) chloride; KCl, potassium chloride.

* Corresponding author.
E-mail addresses: matthewbrucks2025@u.northwestern.edu (M.D. Brucks), alina.arslanova@northwestern.edu (A. Arslanova), CarrieSmith2025@u.northwestern.edu (C.B. Smith), jeffrey.richards@northwestern.edu (J.J. Richards).

https://doi.org/10.1016/j.jcis.2023.05.059
Received 2 March 2023; Received in revised form 19 April 2023; Accepted 9 May 2023
Available online 16 May 2023

Findings: The capping agents installed on the silver shell surface displayed both colloidal stability enhancements and a minimum effective capping concentration that is a function of molecular weight without influencing the shell composition. Particle geometry can be controlled by interchanging the silica template size and shape.

1. Introduction

Engineering the size, shape, and chemistry of silver metal nanoparticles is required to meet the demand for high performance materials used in applications such as precision drug delivery [1], organic molecule catalysis [2], and flexible electronics manufacturing [3]. With silver (Ag) nanoparticle production projected to increase to over 800 tons by 2025 [4], developing new synthesis strategies that control the unique physical and chemical characteristics of Ag metal that emerge at the nanoscale promises to further accelerate their proliferation. Further nanoscale interactions can be dictated by installing molecular architectures that tune interactions of the nanoparticles with themselves and with their surrounding environment [5]. The synthesis of Ag metal nanoparticles is typically carried out in solution by reducing Ag salts in the presence of a suitable capping agent [6]. As the reaction progresses, nucleation and growth occur with the morphology and dispersibility of the resulting Ag particle determined by the details of the reaction and the interaction of a capping agent with the Ag metal surface during the growth phase.

One challenge with this paradigm is the capping agent must play a dual role, both as the structural directing agent, determining the growth rate along different crystallographic planes of the Ag nuclei, and the stabilization agent, ensuring the growing nanoparticle remains stable in the suspending solvent. To enhance stability and size, a noble metal nanoparticle synthesis can be performed in the presence of different surfactants or end-functionalized molecules. As seen in Sakai et al., Pluronic® surfactants were used as both the stabilization and reducing agent for the formation of gold nanoparticles [7]. In this, varying the ratio of the hydrophobic and hydrophilic blocks affected the size distribution, gold precursor conversion, and stability in water. For the titanium dioxide nanoparticles produced by Liao et al., the presence of different ionic surfactants led to changes in particle geometry and size, including spherical, cubic, ellipse, and rod-like geometries [8]. As seen in Li et al. [9] and Chen et al. [10], amine- and carboxylate- terminated alkanes can be incorporated on their own to produce oil stable Ag nanoparticles. In these synthesis platforms, the capping agent played a direct role in multiple properties, which can make it difficult to finely tune nanoparticles for a specific application.

While suitable capping agents have been developed to control structure in both aqueous and nonaqueous syntheses, there are often circumstances that emerge where it is desired that the dual responsibilities of the capping agent be decoupled. A common strategy to achieve this decoupling is the incorporation of multiple capping agents into the precursor solution. As seen in Wang et al., the production of Ag nanoparticles was accomplished by complexing silver nitrate with dodecylamine to solubilize the Ag salt in toluene [11]. The reduction was performed using acetaldehyde in the presence of oleic acid, which served as the capping agent. In this example, dodecylamine served both as a complexing agent and was partially responsible for the stability of the resulting nanoparticle product. Oleic acid was necessary to control crystal growth. Similarly, Bastús et al. combined trisodium citrate and tannic acid to produce monodisperse Ag nanoparticles of varying size, where the tannic acid was added to slow the rate of Ag deposition on seed particles present in the reacting mixture [12]. Other strategies utilize post-processing steps that transform the surface chemistry after the synthesis. Kumar et al. utilized a separate phase transfer step by mixing an aqueous colloid of Ag nanoparticles synthesized from silver sulfate and a solution of octadecyl amine in hexanes [13]. More complicated surface modification agents have been explored like peptides which can be adsorbed to noble metal particle surfaces by displacing the original capping agent used during the synthesis [14]. These examples illustrate the complexity of the dual role of the capping agent in particle synthesis as the surface chemistry cannot always be independently controlled from other particle properties like size and shape while minimizing synthesis difficulty. As a result, the development of flexible synthesis strategies that can harness the interchangeability of the nanoparticle design space while decreasing the interdependence of different particle properties can be highly advantageous because of their enhanced tunability for different applications by improving our ability to select for specific optoelectronic properties [15], control geometry [16], or atomic assembly [17].

Recent work by Chen et al. identified a route to modify an electroless deposition strategy to conformally deposit Ag metal onto silica nanoparticles [18]. In this work, the Ag growth was controlled by the sodium citrate concentration. Because the citrate installs a strong negative surface charge on the growing Ag layer, the resulting particles will only form a homogenous suspension in water. Here, we explore a generalization of the protocol from Chen et al. by enabling the synthesis of core–shell silver-silica nanoparticles (AgSiNP) that are oil-dispersible. We accomplish this by performing the Tollens reduction reaction in the presence of a Pluronic® surfactant and an end-terminated alkylamine. We show that this strategy results in Ag-coated silica nanoparticles that are colloidally stabilized both during the reaction and when suspended in decane after surfactant removal. The flexibility of this synthesis strategy is illustrated by performing syntheses as a function of the number of carbons in the alkylamine and on silica cores of different sizes and shapes. Using this strategy, we show independent control of size, shape, and surface chemistry of the silver metal layer.

2. Materials and methods

2.1. Materials

D-(+)-glucose (ACS reagent), trifluoroacetic acid (TFA) (Reagent Plus, 99 %), ethanol (200 proof, ACS reagent, ≥99.5 %), potassium hydroxide (KOH) (ACS Reagent, ≥85 %, pellets), and tetraethyl orthosilicate (TEOS) (Reagent grade, 98 %), decane (ReagentPlus, ≥99 %), poloxamer 407 (P407) (purified, non-ionic), sodium dodecyl sulfate (SDS) (ACS reagent, ≥99 %), ammonia solution 28–30 % (for analysis EMSURE ACS Reagent Ph Eur), silver nitrate (ACS Reagent, >99 %), oleyl amine (technical grade, 70 %), dodecyl amine (≥99 %), decyl amine (95 %), octyl amine (99 %), hexyl amine (99 %), butyl amine (99.5 %), 1-octanol (ACS Reagent, ≥99 %), 1-octane thiol (≥98.5), 1-dodecanethiol (>98 %), polyvinylpyrrolidone (40 kg/mol), 1-pentanol (Reagent Plus, ≥99 %), and sodium citrate dihydrate (≥99 %, FG) were purchased from Sigma Aldrich (St. Louis, MO). Tin (II) chloride ($SnCl_2$) (anhydrous, 99 % min) was purchased from Alfa Aesar. Methanol (Certified ACS), polyoxylethylene lauryl ether (Brij-35) (30 % Solution), potassium chloride (KCl) (Certified ACS), and 2-propanol (Certified ACS) was purchased from Fisher Scientific (Waltham, MA).

2.2. Synthesis of silica templates

Spherical silica nanoparticles (SiNP) were synthesized using the Stöber process [19]. Particles with diameters of 210(6.3) nm were synthesized using 24.84 mL ammonia and 7.2 mL TEOS dissolved in 200 mL ethanol, stirred at 300 rpm overnight. The particles were washed 3 times with water and centrifuged at 4000 rpm for 50 min and dried in a vacuum oven. Sphere diameter was varied by increasing the ratio of ammonia to TEOS. Silica nanorods (SiNR) were synthesized using the

procedure established by Kuijk et al. [20]. The length of silica nanorods was varied by increasing the amount of TEOS added to the stabilized inverse emulsion of water droplets in 1-pentanol.

2.3. Sensitization of silica nanoparticles

The pretreatment solution was prepared by dissolving 29 mM $SnCl_2$ and 72 mM TFA in a 50v/v% water/methanol solution. Then 10 mg of either SiNP or SiNR were suspended in the sensitization solution using sonication for about 30 min before being washed with water 3 times at 3000 rpm for 15 min [21].

2.4. Preparation of silver reagent

A 400 mM Tollens reagent was prepared using silver nitrate. A 0.1 M KOH solution was added to the solution in 0.25 mL increments until the transparent solution becomes a yellow–brown hue from silver oxide formation [22]. Then ammonia was added in 0.25 mL aliquots until the solution transitioned from yellow-brown to dark brown and then became transparent.

2.5. Synthesis of silver coated silica

After the sensitized SiNP were resuspended in 10 mL of water, 15 mL of Tollens reagent was added to a reaction flask for silver nucleation to occur for 15 min. Meanwhile, a P407 stock solution was prepared so that the reaction medium would be at twice the critical micelle concentration when 1 mL was added. A stock solution of capping agent was prepared in ethanol. Aliquots ranging from 1 mL to 62.5 μL of this stock solution were added to the reaction flask to achieve the desired capping agent concentration in 30 mL of reaction medium. Then a balance of ethanol was added to the reaction flask so the total volume of the reaction medium at this point is 27 mL. After adding 3 mL of a 2.5 M D-(+)-glucose solution to the reaction medium, the system was left to react for 2 h. Then the particles were isolated in a centrifuge at 3000 rpm for 15 min and washed with water, isopropanol, and twice with decane. The particles were then stored in 5 mL of decane.

2.6. Nanoparticle characterization

High resolution scanning electron microscopy (HRSEM) images of the particles were obtained with a JEOL JSM-7900FLV using the lower electron detector with an accelerating voltage of 10.0 keV at a working distance of 10 mm. The HRSEM micrographs were analyzed using a Python algorithm. After taking a list of x and y pixel coordinates, the algorithm identifies the regions that correspond to Ag based on the pixel intensity. The threshold is set by the average pixel intensity for the entire image. The fractional coverage is then calculated based on the pixels above the threshold relative to all the pixels for each particle to determine the distribution. Dynamic light scattering (DLS) was used to measure the hydrodynamic size of the SiNP with a Malvern Analytical Zetasizer Nano ZS and the Malvern DTS1070 folded capillary cells. The SiNP were dispersed in a 5 mM KCl solution and scattering was measured with a 173° detection angle (backscattering). UV–visible (UV–vis) spectroscopy was used to assess particle stability using a Thermo Scientific Evolution 201 UV–vis Spectrophotometer with 2x2 mm aperture. The time evolution of the absorbance spectra was measured from 800 to 200 nm at a scan rate of 600 nm/min at 3-minute intervals for 3 h. The samples were prepared by taking 60–100 μL and diluting with up to 3 mL of decane to achieve an initial absorbance value of approximately 0.3–0.4. X-ray diffraction (XRD) was used to measure the crystal structure of the silver on the nanoparticles. AgSiNP suspensions in decane were loaded into a 1 mm capillary tube from the Charles Supper Company (Westborough, MA) and analyzed on a Rigaku AXTG diffractometer with a CuKα source. A quartz crystal microbalance (QCM) was used to measure the minimum concentration of the amine-terminated capping agents in ethanol that would adsorb to a Ag substrate with an in-situ liquid immersion cell from Advanced Wave Sensors S. L. (Paterna, Spain) in conjunction with a N2PK impedance analyzer (Thornhill, Canada).

3. Results and discussion

3.1. Effect of alkylamine capping agents on silver film morphology

The templated Tollens synthesis established by Chen et al. involves two steps (1) the surface sensitization of a silica template and (2) controlled electroless deposition of a silver precursor onto the surface of the template using glucose with the addition of suitable capping agent. Here, trisodium citrate is replaced with end-terminated short chain alkanes. Using oleyl amine as a capping agent in place of trisodium citrate resulted in significant aggregation during the growth of the Ag layer, indicating that the oleyl amine enhanced the particles' hydrophobicity. It is known that the amine head group can adsorb, as depicted in Fig. 1, to the growing Ag crystal during the electroless deposition process to produce a lipophilic surface [11].

A series of surfactants were evaluated to determine which would allow for the optimal growth of the Ag film and simultaneously enhance the stability of AgSiNP in the aqueous reaction medium. As shown in Fig. S1, three surfactants were tested: ionic SDS, non-ionic Brij-35, and polymeric P407. P407 was the only surfactant that had a minimal effect on the morphology of the deposited Ag as compared to the citrate synthesis while maintaining colloidal stability of the particles during reaction. In contrast, the synthesis with SDS behaved as if there was no capping agent present and Brij-35 surfactant resulted in a distribution of AgSiNP morphologies, with overgrown Ag dominating the isolated product. At the end of the synthesis performed with P407, excess

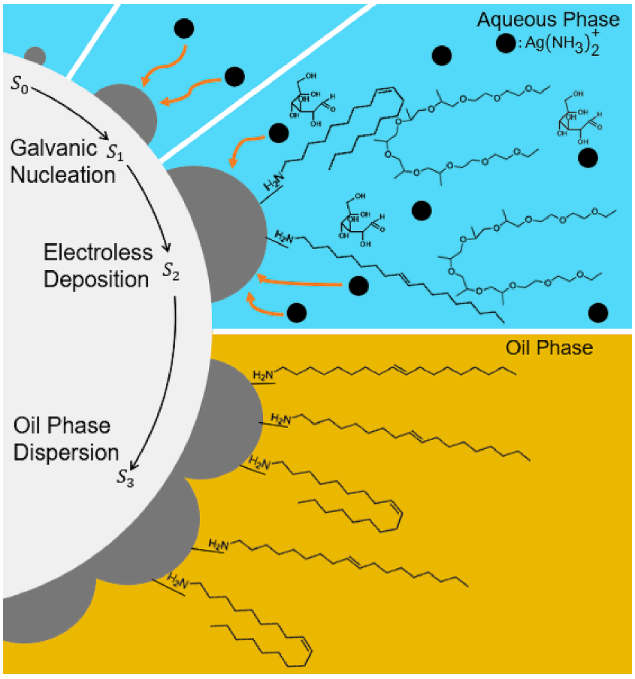

Fig. 1. Oil-dispersible AgSiNP synthesis schematic. An electroless synthesis procedure was adapted to produce oil stable core–shell particles in water. As a pretreatment step S_0, the SiNP are sensitized through the adsorption of Sn^{2+} ions. Then the Tollens reagent is added to seed nuclei across the SiNP surface after undergoing a Galvanic exchange in stage S_1. The Pluronic surfactant and oleyl amine capping agent are then added prior to the addition of the D-(+)-glucose reducing agent to deposit the excess Tollens reagent in stage S_2. In stage S_3, the AgSiNP are isolated from the excess reagents via centrifugation before being dispersed in a nonpolar solvent.

reagents and surfactant were removed by centrifuging in water, isopropanol, and decane, and oleyl amine functionalized AgSiNP were readily dispersible in decane with minimal agitation, indicating that oleyl amine effectively capped the Ag deposition and remained permanently adsorbed.

To understand the influence of the capping agent chemistry on the hydrophobicity of the final product, we compared oleyl amine and oleic acid capped AgSiNP dispersions. Syntheses performed with oleic acid produced particles that were dispersible in water. This is possible if the unsaturated bond adsorbs to the Ag surface leaving a deprotonated carboxyl group exposed to the water, resulting in a negative surface charge on the Ag layer during growth [23]. In contrast, if the amine head group adsorbs head down to the Ag surface, then the alkyl tail is left exposed resulting in a lipophilic surface chemistry. This would allow for the temporary adsorption of the hydrophobic polypropylene block of the P407 to promote the stability of the particle during the synthesis, and its physical adsorption would permit its removal during the isolation stage so that the particles could redisperse in hydrocarbon solvents. The physical adsorption of P407 to a hydrophobic surface is consistent with simulations of Pluronic surfactants which show that adsorption occurs through hemi-micelle formation with the polyethylene oxide blocks exposed to the water phase [24,25].

Once the protocol had been optimized, three qualitative metrics were identified to determine if a synthesis was successful: the AgSiNP should result in a dense Ag film evenly distributed across all the particles in the sample (1), should be temporarily stable in the aqueous reaction medium (2), and be stable in decane after purification (3). Chen et al. demonstrated that the surface morphology of Ag coated SiNP depends on the concentration of the citrate capping agent used to control the growth rate of the Ag film [18]. To explore the effect of capping agent concentration, a similar concentration series was performed over a range of amine terminated alkanes with varying hydrocarbon chain length listed in Fig. 2A.

Starting by varying the length of the alkane tail of the amines, the concentration of each alkylamine was first varied from 1 mM to 0.0625 mM, and then varied from 40 mM to 2.5 mM if the trials at the lower concentration series all failed to produce discrete particles. The resulting Ag film morphologies were examined using HRSEM and are shown in Fig. 2A. Across this concentration range, we observed that the minimum effective capping agent concentration was a function of the molecular weight of the alkyl chains. A transition from effective to ineffective capping was inversely proportional to the length of the alkyl tail, shown in Fig. 2B. We also observed that low molecular weight alkyl amines (<C6) were unable to effectively cap the particles at all concentrations tested. From this survey of capping agents and concentrations, two requirements needed for the alkyl amine capping agents were identified: 1) the capping agent alkyl tail must be of a sufficient molecular weight, and 2) the capping agent must be above the minimum effective capping concentration. Representative HRSEM images of particles that met these criteria are displayed in Fig. 2C.

After evaluating the effect of alkane tail length on the AgSiNP synthesis, the effect of head group chemistry on the synthesis was analyzed. A concentration series was performed for octane thiol, dodecane thiol, and octanol within the expected concentration range given the length of

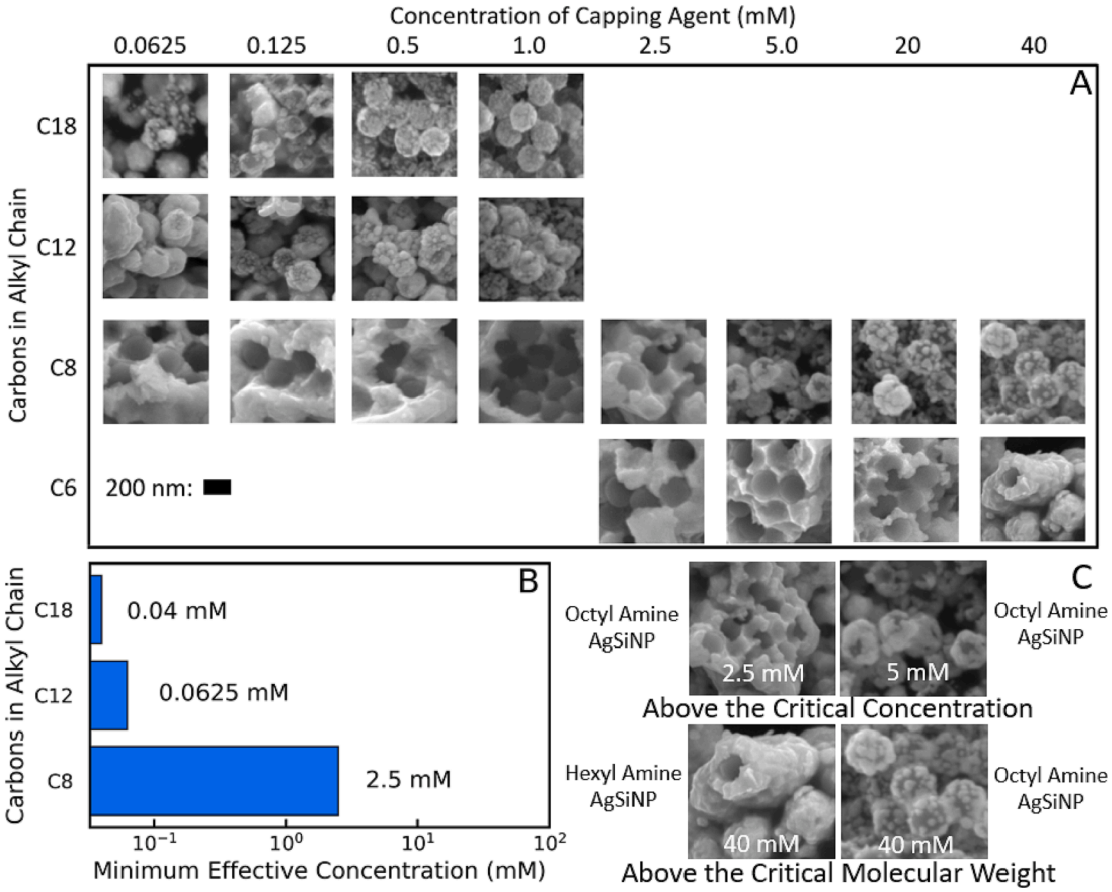

Fig. 2. A) HRSEM images of AgSiNP synthesized with alkyl amines of varying tail length and concentrations in the synthesis medium. The scale bar is 200 nm. B) Bar chart comparing estimates for minimum critical concentration required for effective capping of Ag growth. The values were identified from the image that failed to produce discrete nanoparticles for each capping agent in A. The value for oleyl (C18) amine is estimated from QCM experiments. C) Highlighted comparisons for capping agent design rules for the AgSiNP synthesis. Capping agents must have a sufficient molecular weight and must be above a minimum threshold concentration to successfully limit the Ag deposition process.

the alkyl chain based on the amine syntheses. Neither thiol successfully completed the synthesis, despite known chemistries that use thiol adsorption to synthesize Ag nanoparticles [26–28]. For example, the charge of the thiol group, and thus the pH of a reactive medium, plays a crucial role in the adsorption of thiols to a Ag substrate. As discussed by Gan et al., thiols are only able to adsorb to a Ag substrate after exchanging a proton with a pre-adsorbed citrate, indicating that the thiol group must not have a negative charge [26]. In contrast, our synthesis of oil-dispersible AgSiNPs is performed at a pH ~ 11 from the Tollens reagent preparation, indicating that the thiol group is deprotonated, preventing its adsorption to Ag. The unsuccessful synthesis using octanol as a capping agent can be explained by its poor adsorption at a Ag substrate at room temperature. As described by Zhang et al., short chain alcohol adsorption to Ag requires temperatures below 235 K which are not accessible to our aqueous synthesis protocol [29].

To assess variations in the Ag shell composition due to the capping agent architecture, XRD was performed on AgSiNP suspensions prepared from octyl, dodecyl and oleyl amines. In Fig. 3A, a qualitative comparison of the XRD spectra to the expected peak locations for silver oxide confirmed that no silver oxide was observed in the coating [30]. A further quantification of the peak heights was calculated from the ratio of the facet peak intensity to the corresponding 111 peak intensities to understand if the alkane tail length affected the probability of facet formation. As shown in Fig. 3B, these Ag facet peak ratios remained constant across the three capping agents tested, indicating that the amines undergo a nonspecific adsorption process that is unaffected by the alkane tail. These XRD results, in tandem with our tests of different capping agent head groups, indicate that there is a preferential interaction of the head group with the silver surface that results in an exposed alkyl chain that is responsible for the lipophilic coating observed in the alkylamines.

3.2. Effect of the silica template concentration and shape

To evaluate SiNP loading on the Ag film morphology, syntheses were performed containing the same sized SiNP but with increasing concentration from 0.67 mg/mL to 7 mg/mL. The fractional coverage of Ag on SiNP was measured by analyzing the HRSEM images. Fig. S2 provides an overview of the analysis methodology. In Fig. S2A, the x and y pixel positions of 200 particles were manually selected using ImageJ across four images per formulation. A subimage of each particle was then generated for analysis. In Fig. S2B, a binary intensity threshold was set to differentiate between the pixels that correspond to regions of Ag (green) and regions of bare SiNP (blue). The threshold value was determined using the average pixel intensity of the entire image. This would account for differences in pixel intensity due to variations in the z-height of the particles on the sample holder and construct a distribution of fractional coverage represented in Fig. S2C. This process was then repeated for each AgSiNP formulation to calculate the maximum packing fraction of Ag nuclei on the spherical SiNP surface. From the pixels associated with the identified Ag particles, the area fraction covered was approximated from the average of the distribution.

The Ag coverage on the silica surface decreases after SiNP loadings exceed a 2.5 mg/mL threshold, indicated by the dashed red line in Fig. 4. This systematic decrease in the area coverage corresponds to qualitative changes in the HRSEM images which show a morphology transition from densely packed Ag films to isolated “raspberry” particles. Below the 2.5 mg/mL SiNP loading, the Ag surface remained densely packed, and the morphology was insensitive to the SiNP loading. In this concentration range, an increase in Ag nanoparticles was observed in the first supernatant of the crude reaction product indicating that while all the Ag precursor in the reaction mixture was reduced to Ag metal, not all of that mass was deposited onto the silica surface. The decrease in Ag fractional coverage above 2.5 mg/mL corresponds to what would result if all of the Ag present in the reaction mixture deposited onto the SiNP to form a dense film with approximately 0.9 mean fractional surface coverage. Therefore, the decrease in fractional coverage is explained by a simple mass balance where the total surface area of the nanoparticles exceeds the total amount of Tollens reagent present in the reacting mixture resulting in a decrease in the fractional coverage with increasing SiNP concentration.

To explore the generality of this synthesis strategy on silica templates with different sizes and shapes, the synthesis was performed on spherical and rod-like SiNPs. The spherical template particle diameters used were 210 nm and 315 nm, respectively. Changing particle size was achieved by adjusting the ratio of ammonia to silica precursor during the Stöber synthesis. Silica rods were produced according to the procedure established by Kuijk et al. and rod length was increased through the addition of excess TEOS [20]. In the presence of each of these templates, the synthesis was modified only by changing the template while maintaining the SiNP concentration at 1.25 mg/mL. HRSEM images of the resulting particle morphologies are displayed in Fig. 5. The qualitative appearance of the deposited silver film is the same across all particle geometries. The formation of a dense film across the various silica geometries indicates that this synthesis is robust to changes in SiNP template. Our approach can likely be extended to silica templates with any geometry as the deposition of silver onto silica requires only a negative surface charge to electrostatically adsorb the sensitizing tin cation [31].

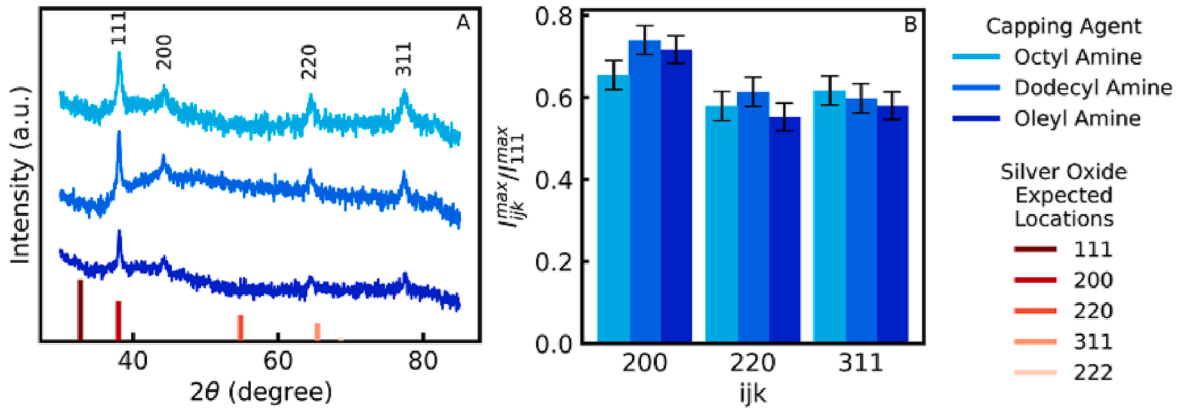

Fig. 3. A.) XRD diffraction peaks for AgSiNP synthesized using octyl, dodecyl, and oleyl amine and suspended in decane. Principle peaks for crystalline Ag are labeled above the expected peak. Characteristic peaks corresponding to the expected locations for silver oxide peaks are labeled in shades of red at the bottom of the spectra to confirm the shell composition. B) Relative peak heights normalized to 111-principal peak for each capping agent that successfully produced AgSiNP. Error bars are calculated from the standard deviation of the baseline noise. (For interpretation of the references to colour in this figure legend, the reader is referred to the web version of this article.)

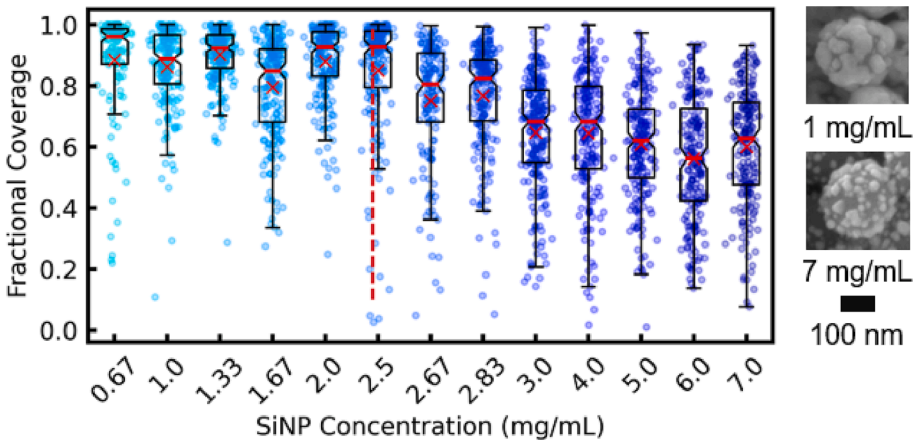

Fig. 4. Fractional coverage for all SiNP concentrations evaluated. The red dashed line corresponds to the threshold calculated from a mass balance for the mass of Ag that can deposit onto a sphere. The red line across each boxplot represents the median of the distribution while the red X on each boxplot represents the mean. The maximum packing fraction for Ag nuclei on SiNP with 210 nm diameters is 0.9. To the right of the boxplots are example HRSEM images of particles analyzed at 1 mg/mL (top) and 7 mg/mL (bottom). (For interpretation of the references to colour in this figure legend, the reader is referred to the web version of this article.)

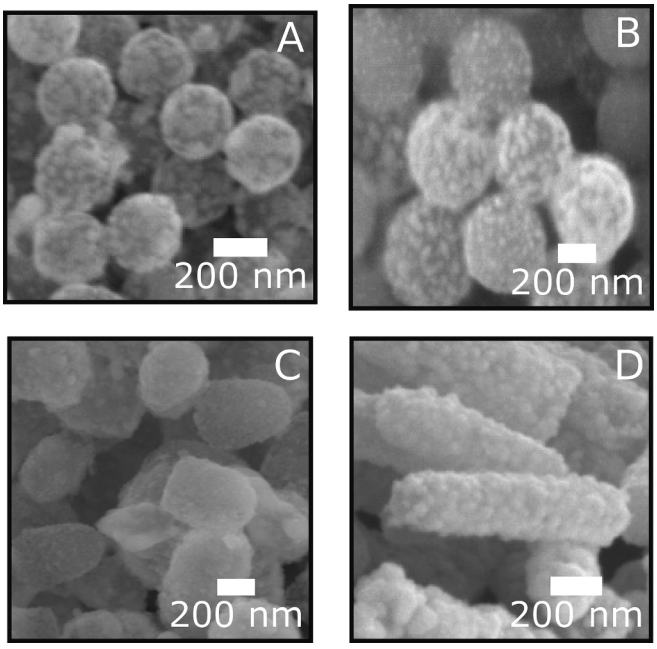

Fig. 5. HRSEM images for morphology comparison of Ag deposited onto various particle geometries and capped with oleyl amine. A) AgSiNP produced from SiNP with core diameter of 210(6.2) nm. B) AgSiNP produced from SiNP with core diameter of 315(6.6) nm. C) AgSiNP produced from silica rod templates with maximum aspect ratio of p ~ 1.7. D) AgSiNP produced from silica rods with maximum aspect ratio of p ~ 8.3.

Further, our results show that, for any template, a simple mass balance can predict the maximum template concentration that can be used to achieve a dense silver shell as shown in Fig. 5A and B. Similarly, an ideal cylinder was used to calculate the threshold concentration of the rods and spheres based on the particle length scales determined from HRSEM. Ag was successfully deposited on the bullet-shaped rods for aspect ratios of p ~ 1.7 in Fig. 5C and p ~ 8.3 in Fig. 5D.

3.3. Quantifying nanoparticle stability using sedimentation.

In all cases where dense silver coverage is observed, the AgSiNPs are readily dispersed in alkanes. To quantify their stability when suspended, we initially explored light scattering experiments, but the optical characteristics of the particles did not permit adequate scattering intensity due to the strong extinction of the particles across all laser wavelengths. Therefore, we performed UV–vis on dilute suspensions of particles in decane. These suspensions were sonicated, and the absorbance was recorded over the course of several hours. During this time, the sedimentation of the particles resulted in a systematic decrease in absorbance intensity across all wavelengths as shown in Fig. 6A for a suspension with oleyl amine as the capping agent. The normalized absorbance values at 500 nm were then fitted to an exponential decay to determine a characteristic time scale for the competing sedimentation-diffusion process described by the Mason-Weaver equation in the SI [32]. For this calculation, the particle density was estimated based on the morphology observed in HRSEM and the assumed Ag nuclei size of 50 nm from HRSEM micrographs in Fig. 2A. The solution to the non-dimensionalized form of the Mason-Weaver equation is a Fourier series that contains an exponential time dependance. The leading order term dominates this Fourier series, and an exponential fit of the early time behavior is shown in the inset in Fig. 6A. The result of this exponential fit is a characteristic timescale, t_c, for the reduction in absorbance. In the early time limit, this timescale can be related to the sedimentation coefficient, s, by dimensional analysis of the Mason-Weaver equation, $s_c = \frac{L}{t_c g}$ where L is the size of the aperture of the UV–vis and g is gravitational acceleration. This expression relates the characteristic sedimentation time to the apparent sedimentation coefficient (s_c) of the particles, which is proportional to the sedimentation velocity.

The sedimentation coefficient of an isolated particle represents the balance of the gravitational force and the viscous drag that the particle experiences during sedimentation. In this experiment, its value depends only on the viscosity of the suspending medium and the particle's

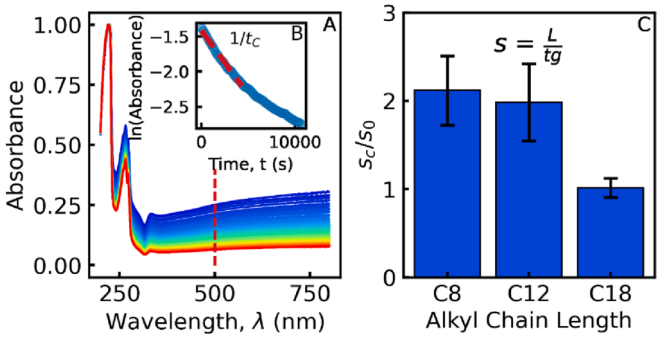

Fig. 6. A) Time evolution of UV–vis absorbance spectra for AgSiNP synthesized with oleyl amine and dispersed in decane. Measurements were made on 3-minute intervals over a 3-hour period B) Linear fitting to early time absorbance values at 500 nm to determine the characteristic time of sedimentation for AgSiNP synthesized with oleyl amine. C) Comparison of average experimental sedimentation coefficient (s_c) for each alkyl amine. The experimental sedimentation coefficient was normalized to the predicted sedimentation coefficient determined from the particle density.

hydrodynamic size. However, the sedimentation coefficient measured at a finite concentration of particles will also be artificially increased as particles aggregate in the suspensions and therefore the difference between the theoretical sedimentation coefficient and the apparent value can be used to assess colloidal stability in our suspensions. For oleyl amine, the average critical sedimentation timescale determined from the UV–vis measurements was 95(12) min. Based on this value, the apparent sedimentation coefficient (s_c) was estimated to be $3.88(41)\times 10^{-8}$ s. To compare this to the sedimentation coefficient of an isolated particle, we assumed a sphere with hydrodynamic radius of 310 nm and density of 6.84 g/cm^3. Using this value, the ideal sedimentation coefficient (s_0) was 3.83×10^{-8} s. The close numerical agreement between the sedimentation coefficients suggests that oleyl amine prevents particle aggregation in suspension and that attractive interactions between particles are minimized. When compared to the other capping agent architectures tests, oleyl amine had the greatest effect on the particle sedimentation rate as shown in Fig. 6C. This indicates that AgSiNP synthesized with longer end-terminated alkanes have a greater stability that more closely matches the predicted value. This agreement is most likely caused by an enhanced solvation effect with the decane. However, despite their dispersibility, all the AgSiNP sediment over a several hour period because of the large density difference and low viscosity of the decane.

4. Conclusions

In summary, we established a robust protocol for the synthesis of lipophilic core–shell nanoparticles by modifying the electroless deposition process of silver onto an inorganic silica substrate at ambient conditions. The deposition of the noble metal onto premade substrates decouples control of particle size and surface chemistry to produce nanoparticles that are dispersible in a solvent with a different polarity than what was used to disperse the synthesis reagents relative to existing literature [11,12]. This synthesis provides a simplified route to obtain lipophilic nanoparticles without the need for high temperatures [10], excess organic solvents [11,33], separate phase transfer steps [9,13], or other deviations from ambient conditions that ultimately limit the applicability and scale-up of the synthesis process while controlling multiple properties simultaneously.

Oleyl, dodecyl, and octyl amines were all used to successfully install a lipophilic surface to the core–shell silver-silica nanoparticles. To prove our hypothesis that lipophilic surface was installed by the head-down adsorption mechanism of these amine-terminated alkanes to the silver surface, we compared different capping agent architectures and their effects on the synthesis outcomes and X-ray diffraction spectra. Performing unsuccessful comparative syntheses using oleic acid, dodecane thiol, octane thiol, and octanol demonstrated that the alkyl tail had minimal effect on the silver shell formation. A further comparison of X-ray diffraction spectra collected for the core–shell silver-silica nanoparticles synthesized with amines of different tail lengths demonstrated that there was no difference in the relative silver peak intensities, indicating that the amine functional group directs the molecular orientation of the adsorption process. This head-down adsorption of the amines would permit the temporary adsorption of poloxamer 407 to the lipophilic surface to temporarily stabilize the particles in the aqueous reaction medium. Once the appropriate capping agents had been identified, scanning electron microscopy was used to determine the experimental parameters, such as optimal and minimum threshold concentrations of the amine-terminated capping agents, to obtain the desired morphologies. A further quantification of the scanning electron micrographs was used to identify the dependence of fractional coverage of silica nanoparticles with the silver film on the silica nanoparticle concentration and to confirm the threshold concentration predicted from a mass balance assuming the formation of a 50 nm thick layer. After maximizing the fractional coverage of the silica nanoparticles by silver, the sedimentation time of the core–shell silver-silica nanoparticles was quantified by recording the evolution of UV–Visible spectroscopy absorbance spectra. Sedimentation rate is greatly reduced by using longer alkane chain amines as capping agents due to an enhanced solvation effect, which allows for particle stability to be tuned based on the ratio of the capping agents used. To demonstrate the versatility of this technique for coating alternative geometries, rod-like silica particles of multiple aspect ratios were successfully used as templates for the synthesis platform. We anticipate the modularity of this core–shell nanoparticle synthesis to further accommodate other core geometries with negative surface charge, core and shell materials, and other capping agents to extend this platform for a variety of applications, such as formulating conductive composites or harnessing the photocatalytic properties of the nanoparticles.

CRediT authorship contribution statement

Matthew David Brucks: Methodology, Investigation, Validation, Visualization, Writing – original draft. **Alina Arslanova:** Methodology, Investigation. **Caroline Bridget Smith:** Methodology, Investigation. **Jeffrey John Richards:** Supervision, Conceptualization, Writing – review & editing.

Declaration of Competing Interest

The authors declare that they have no known competing financial interests or personal relationships that could have appeared to influence the work reported in this paper.

Data availability

Data will be made available on request.

Acknowledgements

This material is based upon work supported by the National Science Foundation Graduate Research Fellowship under Grant No. (DGE-1842165) and Career Award (2047365). This work made use of the EPIC facility of Northwestern University's NUANCE Center, which has received support from the Soft and Hybrid Nanotechnology Experimental (SHyNE) Resource (NSF ECCS-1542205); the MRSEC program (NSF DMR-1720139) at the Materials Research Center; the International Institute for Nanotechnology (IIN); the Keck Foundation; and the State of Illinois, through the IIN. This work made use of the Jerome B. Cohen X-Ray Diffraction Facility supported by the MRSEC program of the National Science Foundation (DMR-1720139) at the Materials Research Center of Northwestern University and the Soft and Hybrid Nanotechnology Experimental (SHyNE) Resource (NSF ECCS-1542205). We would like to additionally thank Qifeng Wang for his assistance in running the amine adsorption experiments with a quartz crystal microbalance in the Department of Materials Science & Engineering at Northwestern.

Appendix A. Supplementary data

Supplementary data to this article can be found online at https://doi.org/10.1016/j.jcis.2023.05.059.

References

[1] M.J. Mitchell, M.M. Billingsley, R.M. Haley, M.E. Wechsler, N.A. Peppas, R. Langer, Engineering Precision Nanoparticles for Drug Delivery, Nat. Rev. Drug Discov. 20 (2) (2021) 101–124, https://doi.org/10.1038/s41573-020-0090-8.

[2] X.-Y. Dong, Z.-W. Gao, K.-F. Yang, W.-Q. Zhang, L.-W. Xu, Nanosilver as a New Generation of Silver Catalysts in Organic Transformations for Efficient Synthesis of Fine Chemicals, Catal. Sci. Technol. 5 (5) (2015) 2554–2574, https://doi.org/10.1039/C5CY00285K.

[3] I.J. Fernandes, A.F. Aroche, A. Schuck, P. Lamberty, C.R. Peter, W. Hasenkamp, T. L.A.C. Rocha, Silver Nanoparticle Conductive Inks: Synthesis, Characterization, and Fabrication of Inkjet-Printed Flexible Electrodes, Sci. Rep. 10 (1) (2020) 8878, https://doi.org/10.1038/s41598-020-65698-3.
[4] S. Temizel-Sekeryan, A.L. Hicks, Global Environmental Impacts of Silver Nanoparticle Production Methods Supported by Life Cycle Assessment, Resour. Conserv. Recycl. 156 (2020), 104676, https://doi.org/10.1016/j.resconrec.2019.104676.
[5] L.Y.T. Chou, K. Ming, W.C.W. Chan, Strategies for the Intracellular Delivery of Nanoparticles, Chem. Soc. Rev. 40 (1) (2011) 233–245, https://doi.org/10.1039/c0cs00003e.
[6] C.V. Restrepo, C.C. Villa, Synthesis of Silver Nanoparticles, Influence of Capping Agents, and Dependence on Size and Shape, A Review. *Environ. Nanotechnology, Monit. Manag.* 15 (2021), 100428, https://doi.org/10.1016/j.enmm.2021.100428.
[7] T. Sakai, P. Alexandridis, Single-Step Synthesis and Stabilization of Metal Nanoparticles in Aqueous Pluronic Block Copolymer Solutions at Ambient Temperature, Langmuir 20 (20) (2004) 8426–8430, https://doi.org/10.1021/la049514s.
[8] D.L. Liao, G.S. Wu, B.Q. Liao, Zeta Potential of Shape-Controlled TiO2 Nanoparticles with Surfactants, Colloids Surfaces A Physicochem. Eng. Asp. 348 (1–3) (2009) 270–275, https://doi.org/10.1016/j.colsurfa.2009.07.036.
[9] D. Li, B. Hong, W. Fang, Y. Guo, R. Lin, Preparation of Well-Dispersed Silver Nanoparticles for Oil-Based Nanofluids, Ind. Eng. Chem. Res. 49 (4) (2010) 1697–1702, https://doi.org/10.1021/ie901173h.
[10] M. Chen, Y.G. Feng, X. Wang, T.C. Li, J.Y. Zhang, D.J. Qian, Silver Nanoparticles Capped by Oleylamine: Formation, Growth, and Self-Organization, Langmuir 23 (10) (2007) 5296–5304, https://doi.org/10.1021/la700553d.
[11] X. Wang, Z. Zhao, D. Ou, B. Tu, D. Cui, X. Wei, M. Cheng, Size-controlled Synthesis of Silver Nanoparticles from Silver Mirror Reaction in Toluene, Micro Nano Lett. 11 (8) (2016) 454–456, https://doi.org/10.1049/mnl.2016.0099.
[12] N.G. Bastús, F. Merkoçi, J. Piella, V. Puntes, Synthesis of Highly Monodisperse Citrate-Stabilized Silver Nanoparticles of up to 200 Nm: Kinetic Control and Catalytic Properties, Chem. Mater. 26 (9) (2014) 2836–2846, https://doi.org/10.1021/cm500316k.
[13] A. Kumar, H. Joshi, R. Pasricha, A.B. Mandale, M. Sastry, Phase Transfer of Silver Nanoparticles from Aqueous to Organic Solutions Using Fatty Amine Molecules, J. Colloid Interface Sci. 264 (2) (2003) 396–401, https://doi.org/10.1016/S0021-9797(03)00567-8.
[14] S.T. Wang, H. Zhang, S. Xuan, D. Nykypanchuk, Y. Zhang, G. Freychet, B.M. Ocko, R.N. Zuckermann, N. Todorova, O. Gang, Compact Peptoid Molecular Brushes for Nanoparticle Stabilization, J. Am. Chem. Soc. 144 (18) (2022) 8138–8152, https://doi.org/10.1021/jacs.2c00743.
[15] Y. Wang, X. Yang, T. Liu, Z. Li, D. Leskauskas, G. Liu, J.B. Matson, Molecular-Level Control over Plasmonic Properties in Silver Nanoparticle/Self-Assembling Peptide Hybrids, J. Am. Chem. Soc. 142 (20) (2020) 9158–9162, https://doi.org/10.1021/jacs.0c03672.
[16] C. Gao, Q. Zhang, Z. Lu, Y. Yin, Templated Synthesis of Metal Nanorods in Silica Nanotubes, J. Am. Chem. Soc. 133 (49) (2011) 19706–19709, https://doi.org/10.1021/ja209647d.
[17] K. Yonesato, H. Ito, H. Itakura, D. Yokogawa, T. Kikuchi, N. Mizuno, K. Yamaguchi, K. Suzuki, Controlled Assembly Synthesis of Atomically Precise Ultrastable Silver Nanoclusters with Polyoxometalates, J. Am. Chem. Soc. 141 (50) (2019) 19550–19554, https://doi.org/10.1021/jacs.9b10569.
[18] J.E. Chen, Q. Wang, K.R. Shull, J.J. Richards, Control over Electroless Plating of Silver on Silica Nanoparticles with Sodium Citrate, J. Colloid Interface Sci. 576 (2020) 376–384, https://doi.org/10.1016/j.jcis.2020.05.024.
[19] W. Stöber, A. Fink, E. Bohn, Controlled Growth of Monodisperse Silica Spheres in the Micron Size Range, J. Colloid Interface Sci. 26 (1) (1968) 62–69, https://doi.org/10.1016/0021-9797(68)90272-5.
[20] A. Kuijk, A. Van Blaaderen, A. Imhof, Synthesis of Monodisperse, Rodlike Silica Colloids with Tunable Aspect Ratio, J. Am. Chem. Soc. 133 (8) (2011) 2346–2349, https://doi.org/10.1021/ja109524h.
[21] Y. Kobayashi, V. Salgueiriño-Maceira, L.M. Liz-Marzán, Deposition of Silver Nanoparticles on Silica Spheres by Pretreatment Steps in Electroless Plating, Chem. Mater. 13 (5) (2001) 1630–1633, https://doi.org/10.1021/cm001240g.
[22] S. Durmazel, A. Üzer, B. Erbil, B. Sayın, R. Apak, Silver Nanoparticle Formation-Based Colorimetric Determination of Reducing Sugars in Food Extracts via Tollens' Reagent, ACS Omega 4 (4) (2019) 7596–7604, https://doi.org/10.1021/acsomega.9b00761.
[23] T. Bala, A. Swami, B.L.V. Prasad, M. Sastry, Phase Transfer of Oleic Acid Capped NicoreAgshell Nanoparticles Assisted by the Flexibility of Oleic Acid on the Surface of Silver, J. Colloid Interface Sci. 283 (2) (2005) 422–431, https://doi.org/10.1016/j.jcis.2004.09.018.
[24] Y. Li, H. Liu, J. Song, O.J. Rojas, J.P. Hinestroza, Adsorption and Association of a Symmetric PEO-PPO-PEO Triblock Copolymer on Polypropylene, Polyethylene, and Cellulose Surfaces, ACS Appl. Mater. Interfaces 3 (7) (2011) 2349–2357, https://doi.org/10.1021/am200264r.
[25] X. Song, S. Zhao, S. Fang, Y. Ma, M. Duan, Mesoscopic Simulations of Adsorption and Association of PEO-PPO-PEO Triblock Copolymers on a Hydrophobic Surface: From Mushroom Hemisphere to Rectangle Brush, Langmuir 32 (44) (2016) 11375–11385, https://doi.org/10.1021/acs.langmuir.6b02414.
[26] W. Gan, B. Xu, H.-L. Dai, Activation of Thiols at a Silver Nanoparticle Surface, Angew. Chemie Int. Ed. 50 (29) (2011) 6622–6625, https://doi.org/10.1002/anie.201101430.
[27] J. Ahn, S. Shi, B. Vannatter, D. Qin, Comparative Study of the Adsorption of Thiol and Isocyanide Molecules on a Silver Surface by in Situ Surface-Enhanced Raman Scattering, J. Phys. Chem. C 123 (35) (2019) 21571–21580, https://doi.org/10.1021/acs.jpcc.9b05383.
[28] C. Kumara, H. Luo, D.N. Leonard, H.M. Meyer, J. Qu, Organic-Modified Silver Nanoparticles as Lubricant Additives, ACS Appl. Mater. Interfaces 9 (42) (2017) 37227–37237, https://doi.org/10.1021/acsami.7b13683.
[29] R. Zhang, A.J. Gellman, Straight-Chain Alcohol Adsorption of the Silver(110) Surface, J. Phys. Chem. 95 (19) (1991) 7433–7437, https://doi.org/10.1021/j100172a059.
[30] S. Gates-Rector, T. Blanton, The Powder Diffraction File: A Quality Materials Characterization Database, Powder Diffr 34 (4) (2019) 352–360, https://doi.org/10.1017/S0885715619000812.
[31] C.H. de Minjer, P.F.J.v.d. Boom, The Nucleation with SnCl2-PdCl2 Solutions of Glass Before Electroless Plating, J. Electrochem. Soc. 120 (12) (1973) 1644, https://doi.org/10.1149/1.2403321.
[32] M. Mason, W. Weaver, The Settling of Small Particles in a Fluid, Phys. Rev. 23 (3) (1924) 412–426, https://doi.org/10.1103/PhysRev.23.412.
[33] P. Uznanski, J. Zakrzewska, F. Favier, S. Kazmierski, E. Bryszewska, Synthesis and Characterization of Silver Nanoparticles from (Bis)Alkylamine Silver Carboxylate Precursors, J. Nanoparticle Res. 19 (3) (2017) 121, https://doi.org/10.1007/s11051-017-3827-5.